UPPSALA
UNIVERSITET

UPTEC F11 050
Examensarbete 30 hp
September 2011

Construction and evaluation of a magnetoresistive ground penetrating radar system

Mikael Blomqvist

UPPSALA
UNIVERSITET

Teknisk- naturvetenskaplig fakultet
UTH-enheten

Besöksadress:
Ångströmlaboratoriet
Lägerhyddsvägen 1
Hus 4, Plan 0

Postadress:
Box 536
751 21 Uppsala

Telefon:
018 – 471 30 03

Telefax:
018 – 471 30 00

Hemsida:
http://www.teknat.uu.se/student

Abstract

Construction and evaluation of a magnetoresistive ground penetrating radar system

Mikael Blomqvist

This Master Thesis examines the possibility to apply a magnetometer developed by the Ångstöm space technology center to a small magnetic ground penetrating radar system with dimension in the order of one dm^3. The magnetometer is broadband (DC-1GHz) and miniaturized. Loop antennas are used to transmit the signal.

A series of experiments have been performed in order to characterize the system, mainly examining the ability to determine distance to a target, using continuous sine wave signals and pulse trains. Standing wave patterns are formed between antenna and target and can be used for determining distance in the continuous case. When using a pulse train, the echo from the target could not be resolved using the current experiment set up, distance could therefore not be determined.

Handledare: Anders Persson
Ämnesgranskare: Hugo Nguyen
Examinator: Tomas Nyberg
ISSN: 1401-5757, UPTEC F11 050

Sammanfattning

Syftet med detta examensarbete är att undersöka huruvida en magnetisk tunnelövergång kan tillämpas på ett magnetiskt markradarsystem. Rapporten behandlar konstruktion av ett experimentsystem samt mätningar med systemet och resultaten av dessa.

Ett markradarsystem fungerar som en vanlig radar, men ger utslag på föremål som är begravda under marken i stället för i luften. Det speciella med en magnetisk markradar är att den är mindre känslig för olika markskikt och resultaten är därför lättare att tolka, men ger samtidigt mindre information. Magnetfältssensorn som används i systemet är utvecklad på Ångström rymdtekniska centrum (ÅSTC) och använder sig av en magnetisk tunnelövergång, där elekroner tunnlar genom en tunn bariär. Tunnlingssannolikheten, och därmed signalstyrkan från sensorn, beror av det omgivande magnetfältets styrka.

Markradarsystemet består av en krets som genererar en kontinuerlig sinusvåg med en frekvens på några hundra MHz som sedan skickas till en antenn. Antennen skickar ut signalen som sedan reflekteras mot ett mål, tillbaka till magnetfältssensorn som sitter placerad i mitten av antennen. Den utskickade signalen bildar tillsammans med den reflekterade signalen stående vågor, då de antingen förstärker eller tar ut varandra på olika avstånd från målet. Magnetfältssensorn mäter styrkan på dessa stående vågor, som varierar periodiskt med avståndet till målet. Ifall det stående vågmönstret för en given antenn är känt, kan förslag ges på möjliga avståndsintervall som målet kan befinna sig i för en mätning. Systemet använder sig av tre antenner som sänder på olika frekvens. Mätningarna på var och en av dessa frekvenser ger olika förslag på målets position, men frekvenserna är valda så att endast ett överlappande intervall föreslås av alla mätningar. Detta intervall anger målets position med en given mätosäkerhet.

Flera mätningar med systemet utfördes för att utvärdera dess prestanda vad gäller upplösning (storlek på mål som kan upptäckas), osäkerhet i positionsbestämning i djupled och sidled, samt möjligheten att upptäcka mål begravda i snö. Endast större mål kunde upptäckas med rimlig noggrannhet, och osäkerheten för dessa var runt 1,8 cm i djupled.

Slutsatsen är att det är möjligt att använda magnetiska tunnelövergångar i ett markradarsystem och dessutom går systemet att göra relativt litet (min-

dre än en kubikdecimeter, exklusive antenn). Mer arbete måste läggas ner på att minimera störningar i systemet. Data från sensorn måste behandlas och presenteras på ett sätt som kan läsas av och förstås direkt av användaren. Dessutom kan det vara bra att prova på fler antenndesigner.

Contents

Chapter 1

Introduction

The scope of this thesis is set to examine the possibility to apply a spin-dependent tunnelling magnetometer (SDTM) to a small magnetic ground penetrating radar (GPR) system. "Small" in this case refers to a system that can fit within a cubic volume of 1 dm^3, excluding the antennas.

A GPR is used to detect signatures of targets buried under ground, much similar to an air radar, although the attenuation in the ground is much higher, which limits the range. A magnetic GPR measures magnetic fields and is therefore not affected by the same attenuation as electric fields [5].

1.1 Ångström Space Technology Centre

The thesis work was conducted at the Ångström Space Technology Centre (ÅSTC). Since it's creation in the year 2000, the centre has been working on implementing microsystems in space applications. The main focus is on increasing performance and cutting costs as well as understanding how the space environment affects miniaturized equipment. [1]

1.2 Spin-dependent tunnelling magnetometer

ÅSTC has developed a microstructured spin-dependent tunnelling magnetometer (SDTM) designed for use on nano-satellites, as well as in fully miniaturized systems for measuring the magnetic field [1]. The magnetometer uses a magnetic tunnel junction (MTJ) [1]. The MTJ consists of two thin ferromagnetic electrode layers separated by a dielectric barrier. This barrier is only a few nanometres thick. A voltage is applied over the barrier via the electrodes, making electrons tunnel through it. The tunnelling probability is dependant on the electron spins. If the magnetization of the two electrodes

is parallel, the spin of the electrons on one side and the electron vacancies on the other are also parallel. The electrons are then likely to tunnel and the resistance is low. The opposite is true if the magnetization of the electrons is anti-parallel [6].

One of the electrodes is magnetised by an exchange-bias magnetic field, and the other is allowed to be magnetized freely by surrounding magnetic fields. The amount of tunnelling electrons thus depend on the magnitude and direction of the applied magnetic field. The tunnelling electrons, i.e. the current through the barrier, constitutes the output signal which is later amplified by supporting electronics. [6]

Compared to other types of magnetometers, the SDTM is competitive when it comes to sensitivity, power consumption, size and mass. It also has a high bandwidth (DC to 1 GHz [2]). Small size, mass and the ability to run from a battery is obvious advantages when designing a hand-held system. The wide bandwidth gives a wider choice of antennas and the high frequency gives the possibility to choose smaller antenna designs, suitable for a hand-held system.

1.3 Ground penetrating radar systems

There are different GPR systems for different purposes. They all have many similarities to radar systems in general, for example, the system consists of an antenna that transmits electromagnetic radiation which is reflected from targets and then received by a sensor [3]. The received signal is processed and the targets show up as signatures [3]. GPRs are usually ultra wide band (UWB), meaning that they cover a wide frequency range. Most systems operate in some part of the region from a few MHz to around 10 GHz, and the bandwidth is typically around one decade (300MHz to 3GHz is a common range) [3].

What ultimately determines the design of a radar system is its intended application. To detect small targets the frequency have to be higher but the range will be limited due to the generally larger attenuation of higher frequencies [3]. The opposite is true if the GPR is designed for detecting larger targets buried deeper down. Different media also have different absorption spectra [3]. Ice has a maximum absorption at around 1 kHz [3], whereas the maximum for water occur in the microwave region [3]. GPRs can generally penetrate granite, dry sand, snow, ice and fresh water, but not salt water [3]. GPRs can detect variations in conductivity, permittivity, [3] and permeability [3] for different materials and layers under ground, all of which will produce a radar signature. However, the magnetic response is usually weaker in most soils [3]. A magnetic GPR is insensitive to changes in permittivity in the near field region. [4], which is where the magnetic

GPR presented in this thesis operates. Because of the cluttered nature of most ground layers, some knowledge of the ground and the expected target to be detected might be required to make sense of the measurements and filter it properly [3].

There are two distinct classifications of radar systems in general and GPRs in particular; systems that transmits a pulse and receive the reflected signal, operating in the *time domain* and system that transmits continuous waves on individual frequencies in frequency domain [3]. In the time domain distances to targets can be estimated by measuring the time it takes the reflected pulse to return, with some knowledge of the propagation speed of the medium [3]. In the frequency domain, for the system presented in this thesis, the amplitude of standing waves can be measured, and the phase of the signal can be determined. If the phase for several frequencies are known, the most likely integer amount of wavelengths can be determined, yielding distance to the target.

Some shielding or filtering between the transmitter antenna and the receiver antenna is usually present [3]. Sometimes the receiver and transmitter antenna is the same [3].

1.4 The SDTM GPR system

As mentioned, many commercial GPR-systems are constructed to operate within a certain environment. Since the scope of this thesis was to investigate how the ÅSTC STDM can be applied to GPR, a magnetic GPR was employed. A GPR system using loop antennas for transmitting was constructed. The advantage of using a magnetic near-filed system is that signatures otherwise not visible can now be detected, since the magnetic near-field is insensitive to changes in permittivity [4], as mentioned in the previous section.

Since the magnetometer together with its electronics was broadband, any frequency in the SDTM's range could be used for transmitting. The system used three loop antennas with different resonance frequencies to maximize the power output. The signature from these three antennas was used to determine distance to a target, within a certain range. The resonant frequencies of the antennas range from around 300 - 500 MHz, which maximized the resolution (what size of targets that could be resolved). The antennas were also electrically shielded and transmitted mainly magnetic near-fields. This thesis investigates the systems performance in two domains, time and frequency. For both cases a radio frequency (RF) circuit was used to feed the loop antennas, and in the pulse case a switch was used to produce a pulse train.

Chapter 2

Theory

The antennas in the GPR system were all operated in the magnetic near-field region. In this Chapter, a brief calculation of the magnetic H-field from a loop antenna is presented. This will be used to motivate the models used in Chapter 4. A description of the mathematical background of deciding distance to objects using orthogonal frequencies is also presented.

2.1 H-field

The H-field from a loop antenna can be expressed by [7]:

$$\overrightarrow{H} = \frac{1}{\mu}\nabla \times \overrightarrow{A}, \tag{2.1}$$

where the vector potential $\overrightarrow{A}$ is expressed in spherical coordinates (r, θ, ϕ) as:

$$A_r(r,\theta,\phi) = -\frac{\mu}{i2\beta r}\frac{d}{d\phi}\mathfrak{T}, \tag{2.2}$$

$$A_\theta(r,\theta,\phi) = -\frac{\mu}{i2\beta r tan(\theta)}\frac{d}{d\phi}\mathfrak{T}, \tag{2.3}$$

$$A_\phi(r,\theta,\phi) = -\frac{\mu}{i2\beta r cos(\theta)}\frac{d}{d\theta}\mathfrak{T}, \tag{2.4}$$

where

$$\mathfrak{T}(r,\theta,\phi) = \frac{1}{2\pi}\int_0^{2\pi} I(\theta')e^{-i\beta\Re'}d\theta', \tag{2.5}$$

$$\beta^2 = \omega^2 \mu \epsilon, \tag{2.6}$$

where $I(\theta')$ is the current distribution in the antenna, μ is the magnetic permeability of the space around the antenna, ω is the frequency of the antenna current, ϵ is the electric permittivity of the space around the antenna [7]. The current varies over the antenna length, since the wavelength used in the experiment was in the same order as the antenna length, but for the purposes of this calculation, it can be assumed to be constant, since it is the field magnitude dependence on distance that is of interest.

When Eq. 2.1 is evaluated for an antenna radius a, it can be noted that the magnitude of the magnetic field exhibits a $r^{-2}(r^2 + a^2)^{-1/2}$ dependence on distance from the antenna. This expression approaches r^{-3} a few radii from the antenna.

2.2 Orthogonal frequencies

As mentioned before, the radar system, in one case, uses orthogonal frequency signals to determine the distance to a target. By determining the phase of the three signals, the number of wavelength from the source can be determined. The orthogonality is valid over a certain distance. This theoretical maximum distance (b_{max}) is calculated by considering the wavelength of the three signals, λ_1, λ_2 , λ_3, and finding the smallest values for an integer n, so that the following holds true for some integer i

$$i\lambda_1 = n\lambda_2 \tag{2.7}$$

and then finding the smallest integer m so that

$$mn\lambda_2 = i\lambda_3 \tag{2.8}$$

for some integer i.

The maximum distance is then:

$$b_{max} = mn\lambda_2 \tag{2.9}$$

However, in practise one would want the possible set of phase differences to exceed some length Δ_λ for the desired range $d = m_m n_m \lambda_2$.

For any two sets of values n_1, m_1 and n_2, m_2, $(n_1, n_2 < n_m), (m_1, m_2 < m_m)$, the following should hold true for any integer i_1, i_2:

$$max(|(i_1\lambda_1 - n_1\lambda_2) - (i_2\lambda_1 - n_2\lambda_2)|,$$

$$|(n_1\lambda_2 - m_1\lambda_3) - (n_2\lambda_2 - m_2\lambda_3)|) > \Delta_\lambda, \forall n \in \mathbf{N} < n_m \tag{2.10}$$

For the system presented in this thesis, b_{max} is in the order of a few meters, which is in the operating range of the radar.

Chapter 3

Experiment

All experiments within the thesis were done using the same basic experiment setup consisting of two main parts; a transmitter, consisting of shielded loop antennas, RF-circuits for feeding the antennas, and a receiver, containing the SDTM and an amplifier circuit. All was mounted on a mobile cart. For some parts an oscilloscope was used to record the data and a digital to analog converter (DAC) to control the system. The measurements were done using both continuous waves and pulse trains.

3.1 Continuous Wave Measurements

3.1.1 Experiment Setup

The system used for the continuous wave measurements consisted of a RF-circuit (RF-circuit A, see figure 3.1) with the amplifier connected to the loop antenna and a constant voltage signal source connected to the oscillator, either a battery with a voltage divider or the DAC, which determined the output frequency. The receiver was the ÅSTC SDTM integrated on an electronic circuit, connected to a logarithmic amplifier. The logarithmic amplifier output a signal proportional to the power the sensor received over a broad frequency spectra covering all signals from the loop antennas. This system is hereafter referred to as the "continuous wave measurement system"(CWMS). Below is a brief listing of the system components used (see Fig. 3.1):

MATLAB:
A MATLAB script controlled the system by sending instructions to the DAC (see program listing in Appendix A).

DAC:
This device transformed the computer commands to an analogue output

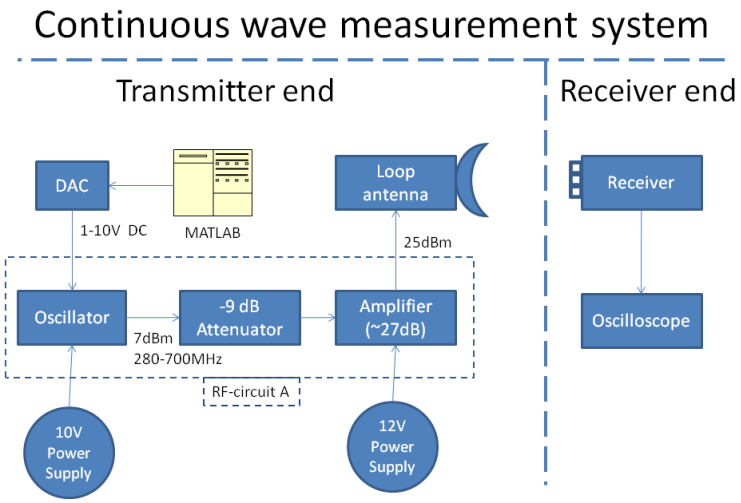

Figure 3.1: Schematic view of the continuous wave measurement system.

voltage that was sent to the oscillator.

RF-circuit A:
This is a gathering name for the three next items bellow used for reference later. See figure 3.3 and figure 3.1

Oscillator:
Outputs a single frequency sine signal that varies with input voltage. It was controlled by the DAC voltage (product number: ZX95-625+, Mini-Circuits, USA).

-9dB attenuator:
Attenuates a signal by 9 dB. It received the 7 dBm signal from the oscillator and matched it with the amplifier maximum output power after amplification of the signal (product number: VAT-9+, Mini-Circuits, USA).

Amplifier:
Amplifies a signal with 27 dB, capped at 25 dBm (about 300 mW). The -2 dBm signal from the attenuator was amplified to the cap level of 2 dBm (product number: ZRL-700+, Mini-Circuits, USA).

Loop antenna:
A coaxial cable that formed a circle. Both the inner and outer connectors at one end were soldered to the outer connector so that it closed on itself to form a circle. There is also a slit in the coaxial cable that prevent currents from flowing along the circle, see Fig. 3.2. For all experiments three antennas with different radii were used: 13, 17 and 23 cm (hereafter re-

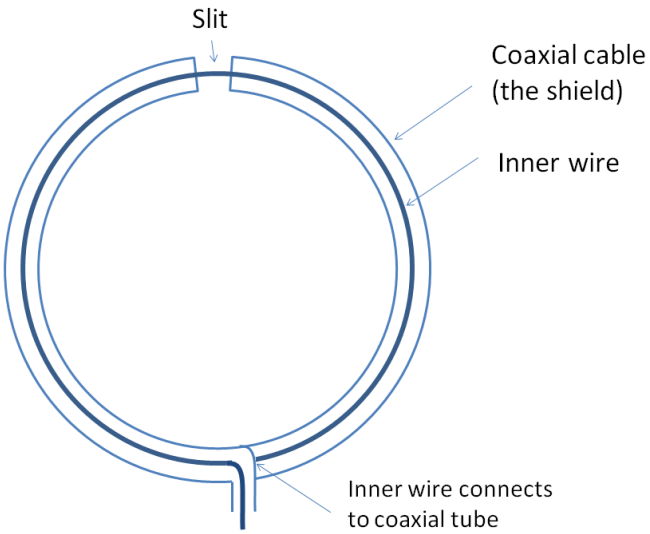

Figure 3.2: Loop antenna with slit.

ferred to as small, medium and large antenna, respectively). The antennas were mounted coaxially and connected to the rest of the system one by one throughout the course of the experiments.

Receiver:
Attached coaxially with the antennas, a few millimetres out of the antenna plane, see 3.4. This unit was made up by the ÅSTC SDTM sensor and a logarithmic amplifier. The amplifier produced a output signal proportional to the total power feeded to it.

3.1.2 Calibration

To correlate the output frequency of RF circuit A to the tuning voltage of the oscillator in the RF-circuit, a calibration setup was constructed. The calibration setup was connected in accordance with Fig. 3.5. This setup is essentially the transmitter part of the CWMS but with the antenna replaced with a -10 dB attenuator and an Oscilloscope.

The following paragraph provides a description on how the calibration system works: The MATLAB program (Appendix A and Appendix C) controls the system by instructing the DAC to send a tuning DC voltage to the control port of the oscillator, via the -9 dB attenuator, and the oscilloscope measures the peak frequency output from the amplifier, via the -10 dB attenuator (product number: VAT-10+, Mini-Circuits, USA), and sends the reading back to the program. The last (-10 dB) attenuator is not a part

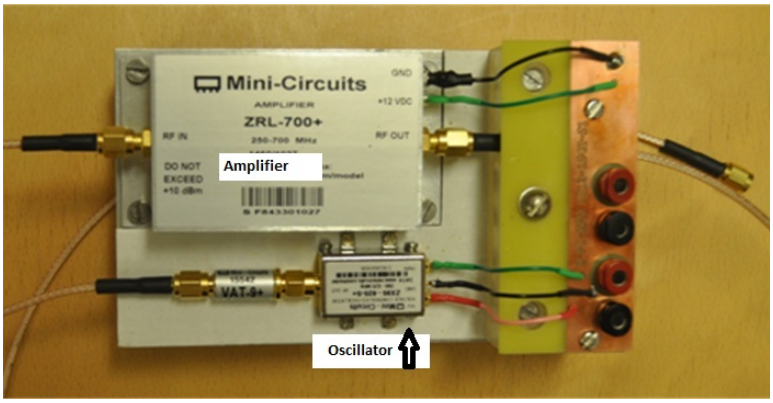

Figure 3.3: RF circuit A.

Figure 3.4: Measurement antennas with sensor in the middle.

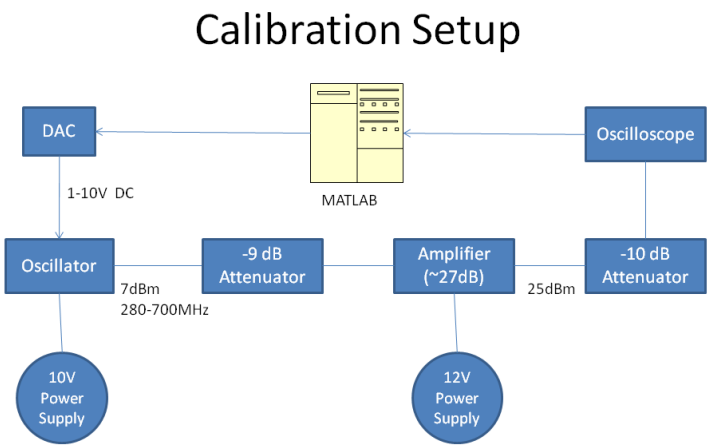

Figure 3.5: Schematic view of the experiment setup.

of the CWMS, but was used to protect the Oscilloscope. The attenuator is a completely passive devise and will not cause any frequency dispersion to the signal.

The calibration was done by increasing the tuning voltage from 0-10 volts and reading the corresponding frequencies. A least mean square polynomial fit was then performed, and the resulting polynomial was stored so that it could be used to correlate the desired frequency to the DAC voltage in upcoming measurements.

The calibration gave an actual verification that the system was transmitting on the desired frequencies. This was useful for creating stable and reliable measurements.

3.1.3 Basic tests

Some basic tests were done on the CWMS without the logarithmic amplifier, using the oscillator to measure the output power of the most powerful frequency peak received by the sensor. Not using the logarithmic amplifier gave a verification that the SDTM sensor produced a useful signal. A target was placed in front of the antenna, and the idea was to measure the variation in signal strength as the target was moved and standing wave patterns was formed between the antenna and the receiver. These tests were done in order to:

- **Verify that standing wave patterns could be detected.**
  The "distance to target" refers to half the distance between the antenna, target and back to the sensor, along a line, coaxial with the antennas. This is true for all measurement. The target used was a 60 cm square steel plate.

- **Verify that the system output a stable frequency.**
  At lower frequencies (200-350 MHz) there were some minor unwanted frequencies super-positioned in the signal, but the signal was still regarded good enough. At higher frequencies the signal was more sinusoid.

- **Characterise the antennas**
  Antenna measurements were done with a network analyser, which gave the resonance frequencies for the antennas. At the resonant frequencies, there is little reflection of a RF signal entering the antenna and most of the energy is radiated.

The system worked well, and standing wave patterns were detected, as intended.

3.1.4 Shielding

The SDTM electronics was shielded from the antenna and other noise sources with a shielding enclosure, formed by the ground plane of the circuit board and a shielding box (product number: PFL11T, Perancea ltd., Great Britain); see Fig. 3.6. Likewise, the magnetic sensor was shielded from the magnetometer electronics. Measurements conducted on the CWMS indicated a reduction in noise of 18.5 dB at the peak power frequency (where most of the noise was).

The sensor was also shielded from the antenna using a μ-metal cylinder, see Fig. 3.7. The μ-metal cylinder prevents electric and magnetic radiation from reaching the sensor from any other direction than the opening, perpendicular to the open ends, thus effectively shielding it from the direct antenna radiation. The shielding also narrowed the field of view of the radar. The attenuation of the direct antenna radiation was in the order of 2-5 dB.

Measurements of the standing waves were performed on the system with and without shielding. The standing wave measurement was done by varying the distance between the antenna and a target from 10 cm to 2 meters, in 5 cm intervals. The target used was a square steel sheet with a side of about 50 cm.

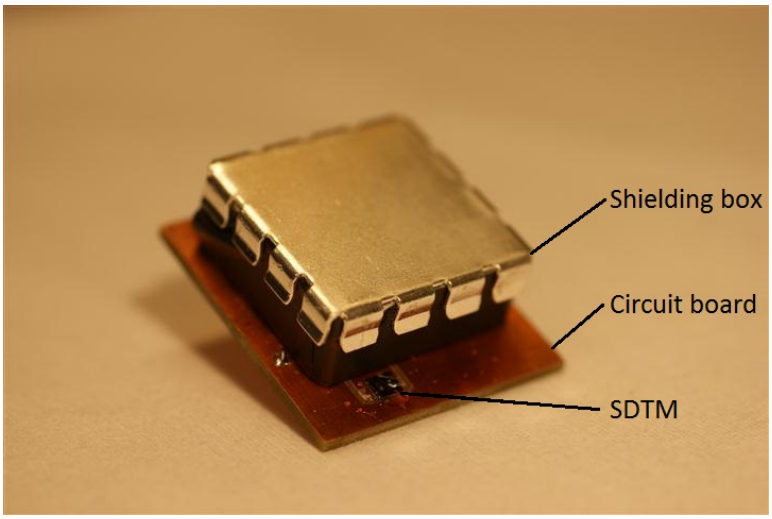

Figure 3.6: Magnetometer circuit board with shielding box.

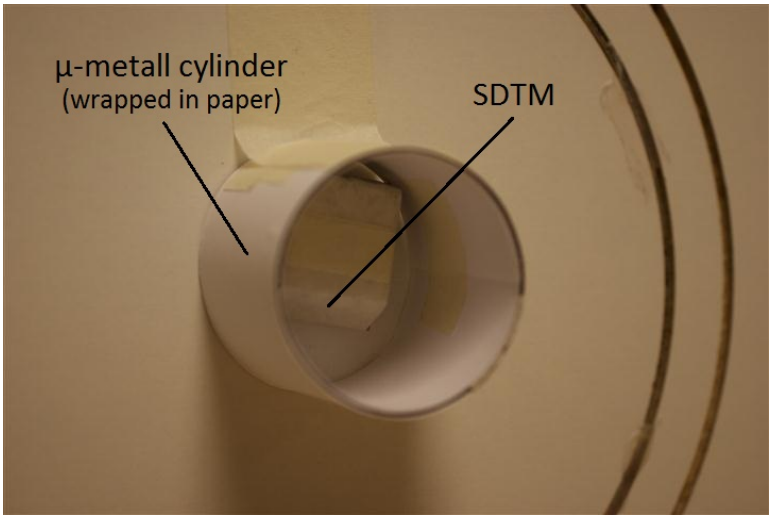

Figure 3.7: Rolled up μ-metal, wrapped in paper, surrounding the magnetometer and electronics.

3.1.5 Standing wave measurements

The CWMS was used for the standing wave study. A MATLAB script controlled the DAC and recorded data from the oscilloscope, see Appendix A and Appendix B

The logarithmic amplifier output a constant voltage that corresponded to the time average power that was recorded by the SDTM from a broad band of frequencies. In this case, the power was dominated by the antenna frequency, which could be verified by turning of the antenna and measuring the voltage. The output signal from the logarithmic amplifier was 1.3 V when there was no signal from the antenna and decreased roughly linearly with increasing signal power.

Numerous different measurements were done at different locations. These were then used as the basis for measurement sequences that were implemented for the depth measurements.

3.1.6 Depth measurements

Depth measurements were performed on radar targets according to a specified measuring sequence. Here different size targets were studied at different distances and orientations with respect to the measurement system. All possible combinations of measurements could not be done because of the limited time of the project, so only distance variations coaxially with the antennas was done for all targets. The Nyquist Theorem was used to choose the step length between measurement points. The Nyquist Theorem gives the maximum distance between sample points to fully describe a signal known to be a superposition of sine waves, given a maximum frequency of the latter. Considering noise and redundancy, and also the practicality of simple integer numbers, 5 cm was chosen as the measurement interval.

A total of 13 different targets were used. They were all 2 mm thick circular steel sheets, 8 with varying sizes and 5 (27 cm in diameter) with varying amount of holes in them. See Tab 3.1

The depth measurements followed three measurement sequences varying the distance from the system to the target in two dimensions.

Sequence 1: The target was moved coaxially from the antennas. The plane of the target surface was perpendicular to the coaxis. The distance from sensor varied from 10 cm to 200 cm, in 5 cm intervals.

Sequence 2: The target was moved perpendicular from the coaxis (also horizontally) at distances 50 cm, 100 cm, 150 cm; in 10 cm steps within the intervals specified in Tab. 3.2.

Table 3.1: Radar targets.

Target name	Diameter [cm]	holes [% of surface]
T05	5	0
T08	8	0
T13	13	0
T20	20	0
T27	27	0
T36	36	0
T45	45	0
T54	54	0
H10	27	10%
H20	27	20%
H30	27	30%
H40	27	40%
H50	27	50%

Table 3.2: Sequence 2.

At the concentric distance from sensor:	distance interval perpendicular to concentric line (10 cm steps):
50 cm	0-80 cm
100 cm	0-160 cm
150 cm	0 - 240 cm

Sequence 3: The target is rotated from 0-90° from the coaxial orientation, in 15° steps, at the distance 50 cm from the sensor.

Measurement sequences used for the depth measurements

For the depth measurements, sequence 1 was repeated for all targets, sequence 2 and sequence 3 was only performed for the target T27. The sequences were only conducted for the small and medium antenna, whereas the large antenna only was used for target T54.

3.1.7 Vertical Plane Measurements

The measurements were performed by moving the T45 target in a vertical plane in front of the antenna. The measurements were done at single points in a grid pattern. Here, the DAC was replaced by a voltage regulator and the output signal was recorded using a volt meter.

The first measurement was done using this system. The resolution of the voltmeter proved to be too low (only 5-7 discrete values was recorded during the course of measurement), so a simple amplifier was built to amplify the output signal about one order of magnitude. A second vertical plane measurement was done using this system.

3.1.8 Snow Measurements

These measurements were performed outdoors with the same measurement system as in the second vertical plane measurement, with the amplifier and a voltmeter. The small antenna was placed in front of a wall of snow and the T54 target was inserted in the snow at various distances ranging from 10 cm up to 160 cm, in 10 cm intervals.

The purpose if these measurements was to show that the magnetic GPR-system indeed penetrated snow.

3.2 Pulse Measurements

The measurement system used for the pulse measurements consisted of the CWMS with a switch (product number: ZFSW-2-46, Mini-Circuits, USA) connected between the amplifier (in the RF circuit) and the antenna. The switch was controlled by a signal generator that sent out 20 ns pulses at 100 μs intervals. For the duration of the pulse, the switch let through the signal from the RF-circuit (the rise time was fast in relation to the pulse length). The pulse signal was then send to the antenna. The purpose of the pulse measurement was to investigate if the transit time of a reflected pulse could be measured by the system.

The pulse was received by an oscilloscope from the sensor. The Oscilloscope was triggered by the pulse from the signal generator. The pulse was about 150 ns long, which corresponds to about 45 meter travel time in air.

The next step in evaluating whether or not a shift of the pulse can be seen with a target at different distance, was to record the oscilloscope curve 100 times and then compute an average.

To improve the signal-to-noise ratio of the measurement an average of 100 pulses was recorded by the oscilloscope and the data saved on a flash disk. This procedure was repeated with and without target and also with the logarithmic amplifier used in the CWMS as well as one from Mini-Circuits. To maximize the resolution, recordings were done with the oscilloscope in 20 ns intervals over a span of 100 ns (to increase the time resolution). Hence, there were discontinuous jumps in the data at 20 ns intervals.

Chapter 4

Results and Discussion

4.1 Continuous Wave Measurements

Some qualitative results can be noted from the standing wave measurements:

- For sequence 1 measurements on T## (## denotes all target sizes), the standing wave pattern becomes clearer as the diameter of target increases. T27/T36 and upwards gave distinct results, see Fig. 4.1. For T36 and upwards, there was less variance from the calibration curve then that of the data itself ($R^2 > 0$). The data from these measurements was linearly offset so that the average value equalled the average of the calibration curve (Fig. 4.9) and also so that the average distance from the average (proportional to amplitude) matched that of the calibration curve. The idea was that the amplitude decreases with target size, and only the shape of the curve, relative to its amplitude should be compared to the calibration curve. Also, the average for each measurement was slightly different because of different conditions with battery voltage, cable positions, etc.
- For sequence 1 measurements on H##, the amount of holes in the material seems to have little effect on the R^2 value, see Fig. 4.2. The 10% holes seem to have lower R^2, but this is likely to be a random variation. The R^2 was calculated with the same method as above.
- For sequence 2 measurements, a standing wave pattern could be seen from moving the target sideways.
- Rotating the target was equivalent to reducing the cross section, see Fig. 4.3. The signal went to the no-target level as the angle approached 90° (The angle- and sideways measurement voltage can not be correlated to the other measurements since the logarithmic amplifier was altered between).

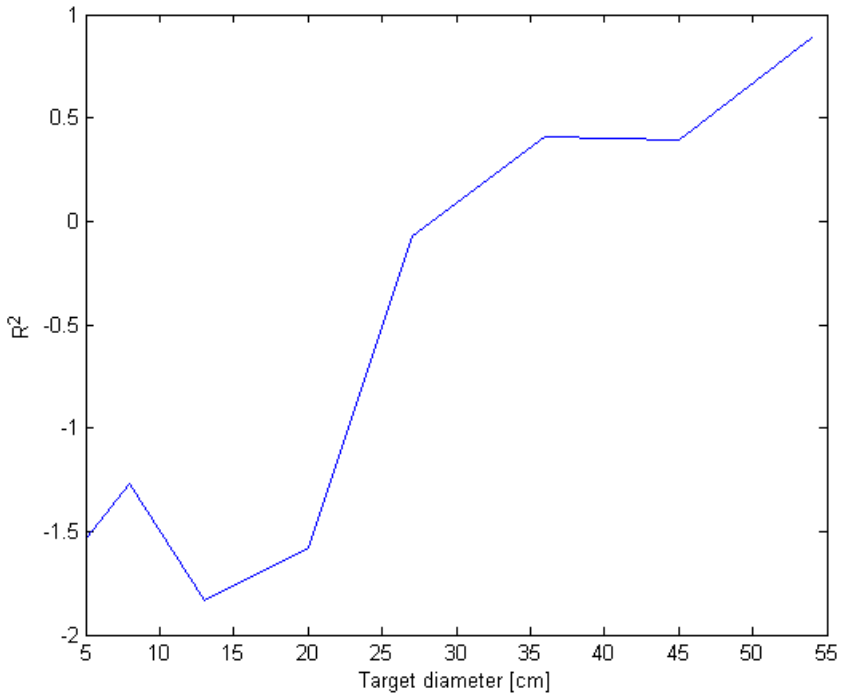

Figure 4.1: R^2 for different size targets

4.1.1 Basic tests

The frequency response of the antennas measured by the network analyser can bee seen in Fig. 4.4. The resonance frequencies used in subsequent measurements were 490.2 MHz for the small antenna and 331.3 MHz for the medium antenna. For the large antenna 343.9 MHz was used.

The results of the basic tests using the CWMS without the logarithmic amplifier, and with the oscillator to measure output power can be seen in Fig. 4.5. Notice that the range in power was in the order of 3 dB for the extremes at lower distances.

4.1.2 Shielding

The shielding experiment was plotted in two graphs, showing the standing wave patterns produced, with and without shielding, see Fig. 4.7 and Fig. 4.6 respectively. Comparing the two figures clearly indicates that the pattern was less affected by noise in the shielded case. The second peak was less distorted. This was an indication that the shielding had a positive effect.

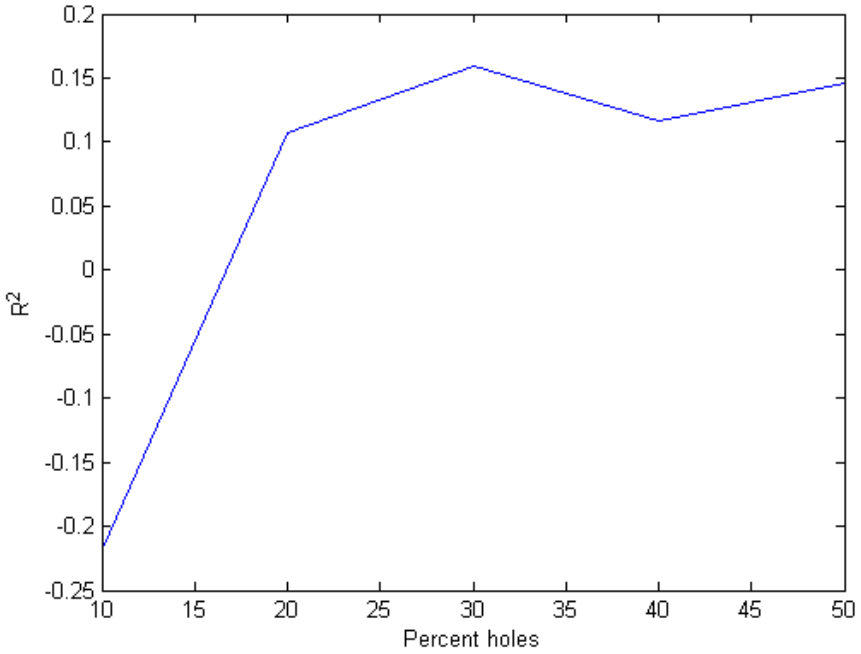

Figure 4.2: R^2 for different amount of holes

4.1.3 Calibration curves

For the CWMS, the distance to a target could be determined using a signature (measurements for one target at a specific distance) and comparing it to calibration curves for the three antennas. Creating calibration curves required some curve fitting.

From the theory chapter, it is clear that the H-field decreases with r^3 in the near-field region and the measurement data suggested that the standing wave pattern had a sine wave shape (see Fig. 4.8 and Fig. 4.9). Therefore, the following model was assumed to provide a good fit,

$$a\sin(2\pi x/l + b)/(1 + (x/c)^3) + d, \tag{4.1}$$

where b is an offset to the phase, d is a voltage offset, a is the amplitude of the curve close to the antenna and l sets the wavelength. The parameter c determines a characteristic distance for the rate of amplitude decrease as distance increases. The denominator $1 + (x/c)^3$ sets the maximum value of the amplitude to a. Finally, x is the distance to target.

A least square fit using the data from sequence 1 measurements on T54 for all antennas, and fitting to Eq. 4.1, using parameters, *a, b, c, d, l*, gave the

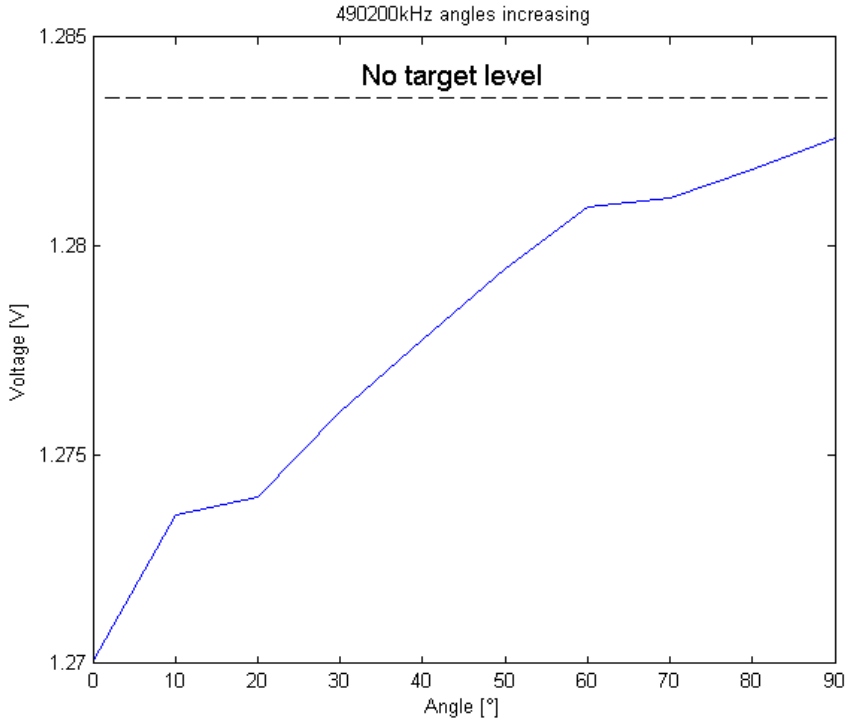

Figure 4.3: Rotating the 27 cm target

calibration curves in Fig. 4.8. Here, l has been allowed to vary 10 % from its theoretical value for vacuum, due to uncertainties in the measurements. Notice that the target distance has to be doubled to get the distance travelled by the reflected wave. Therefore, the theoretical value is half the vacuum wavelength for the frequencies of the respective antennas. The value can then be expressed as (ν is frequency, v_c is light speed in vacuum):

$$l = \frac{v_c}{2\nu}(1 \pm 0.1) \tag{4.2}$$

After the initial fit, for each antenna wavelength (λ_i), a ratio c_i/λ_i (where c_i is the parameter c for each antenna i) was calculated and then the average of these ratios was calculated. The parameter c_i was then changed so that c_i/λ_i equalled this average ratio. Finally, c was allowed to vary by 10% also for the second fit (Fig. 4.8 and Fig. 4.9).

The calibration curves could be improved for a certain range if only the data points for e.g. 25-120 cm were included, see Fig. 4.9

The *rmse*-value is the root of the variance of the data points from the fitted curve. This data can be used to estimate what uncertainness can be expected in distance measurements.

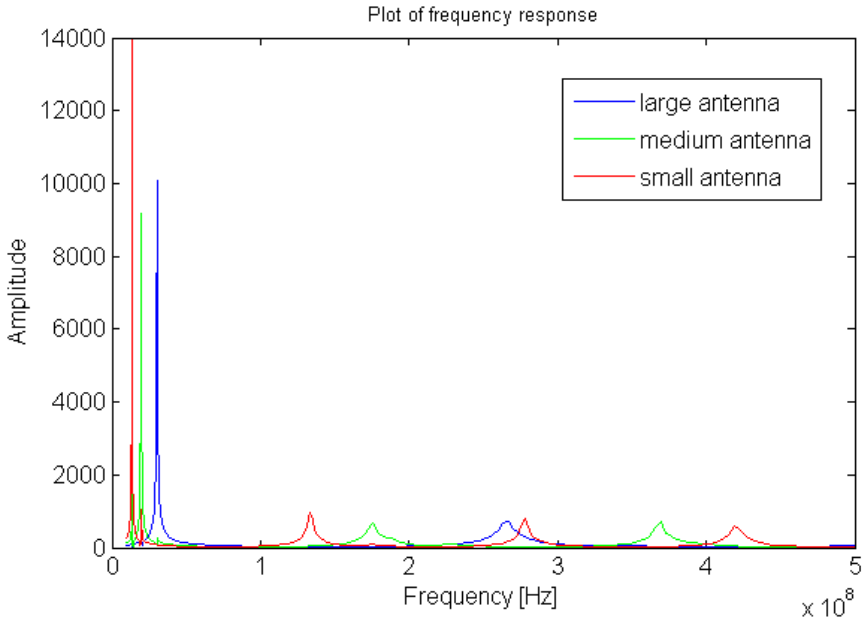

Figure 4.4: Frequency response from the antennas, measured by a network analyser.

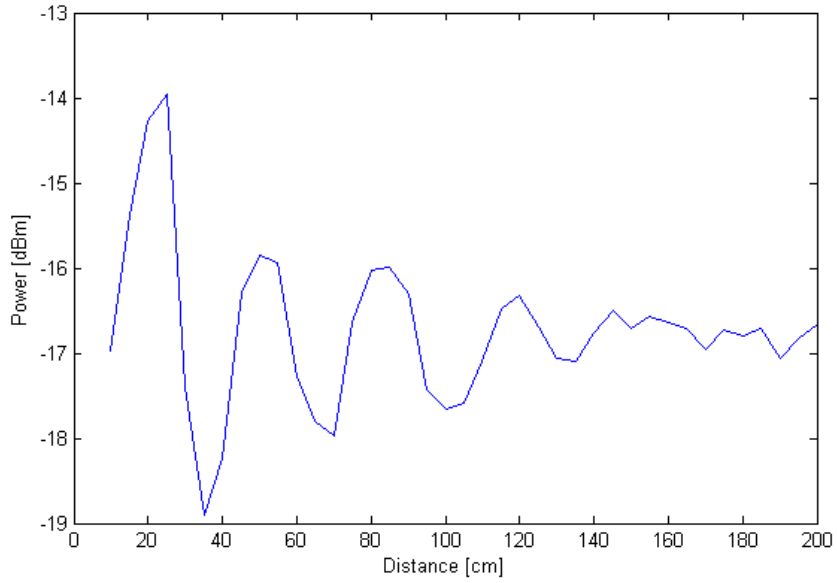

Figure 4.5: Standing wave pattern from measurement on a 60 cm square steel plate

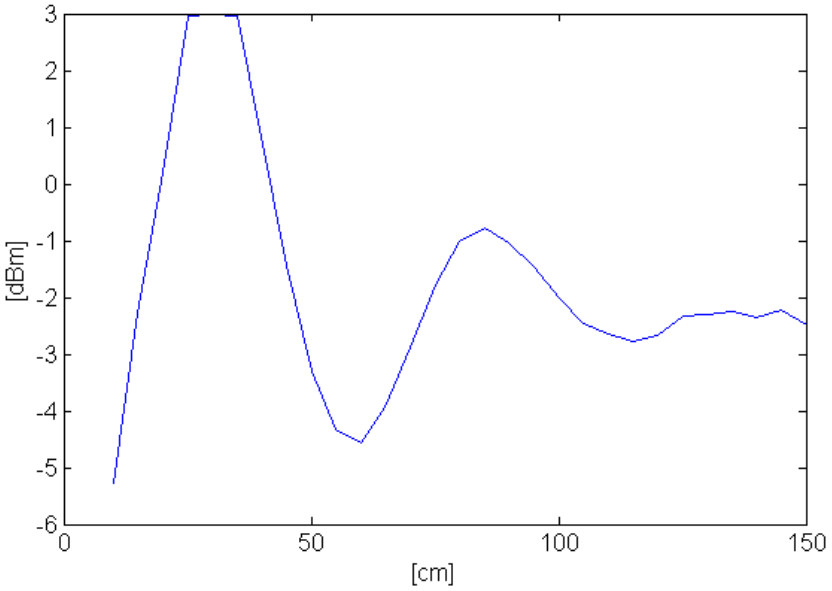

Figure 4.6: Medium size antenna, 331.3 MHz, shielded.

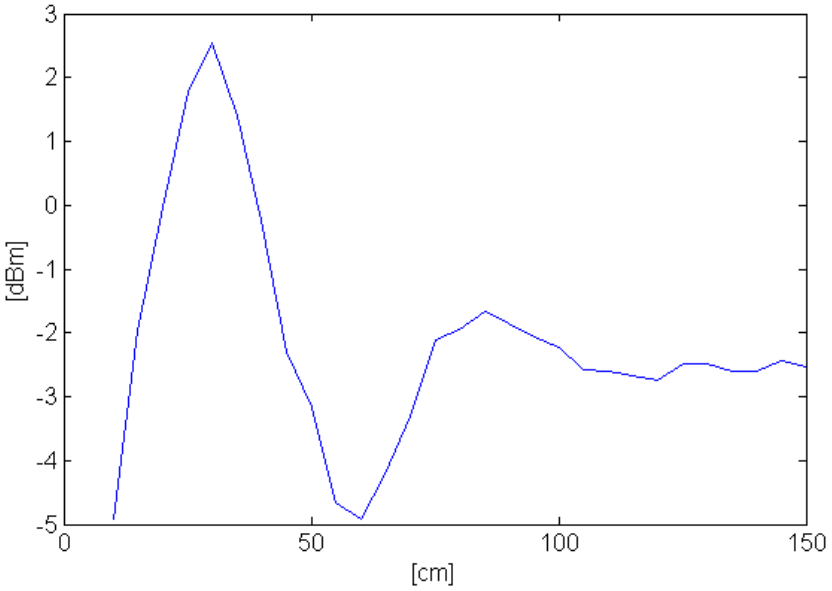

Figure 4.7: Medium size antenna, 331.3 MHz, unshielded.

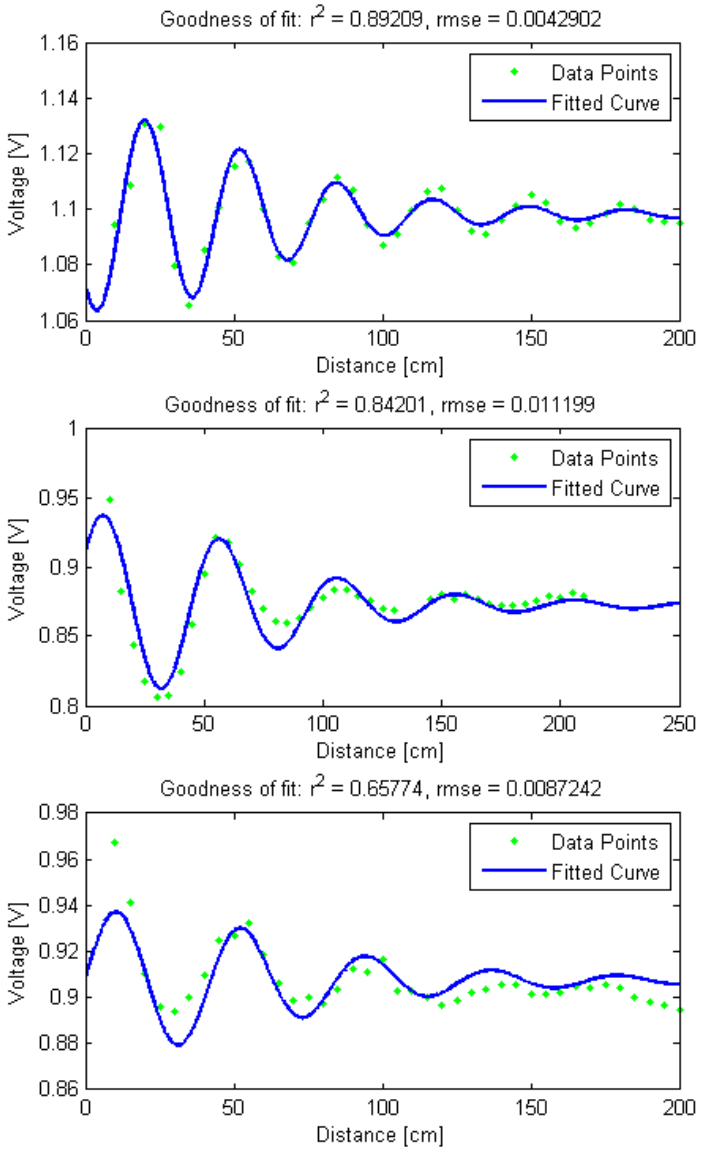

Figure 4.8: Fitted calibration curve and data points

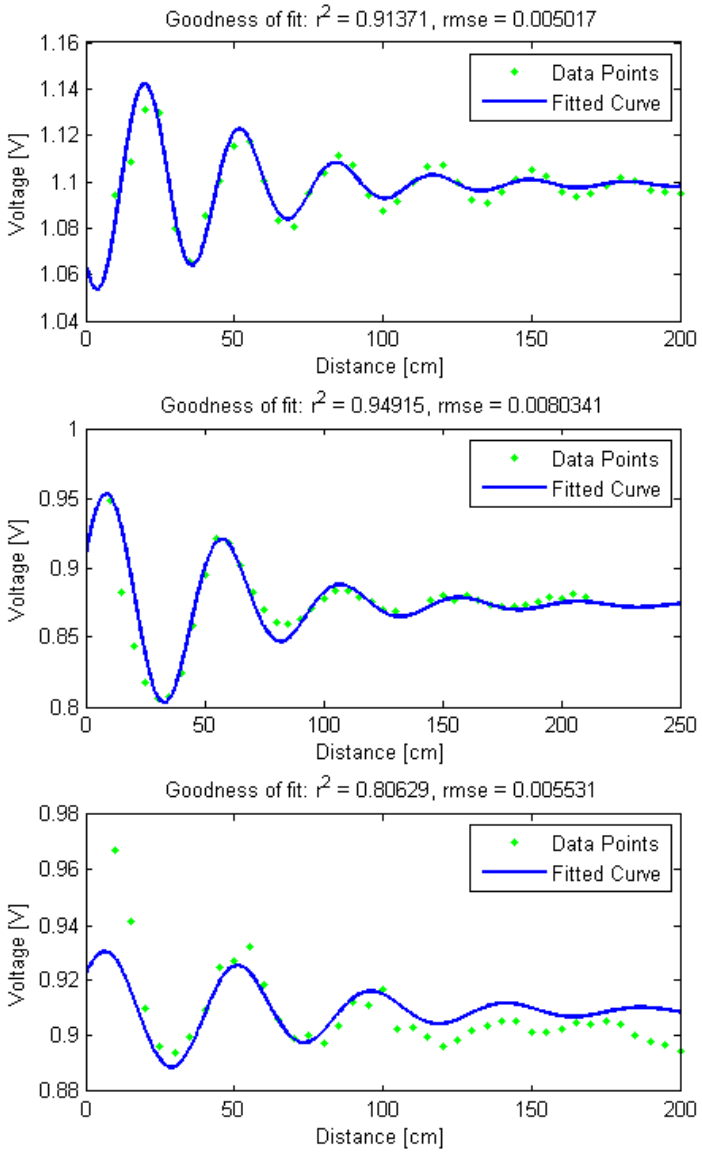

Figure 4.9: Fitted calibration curve and data points

Table 4.1: Distance estimate for sequence 1 measurements on T54

Distance[cm]	Estimate[cm]	% of average
25	25.8	7.90%
30	30.8	0.42%
35	36.1	0.14%
40	40.3	3.53%
45	44.4	2.76%
50	48.9	0.91%
55	54.8	1.81%
60	59.7	0.33%
65	65	0.42%
70	68.9	0.62%
75	72.5	3.52%
80	75.9	5.05%
85	87.6	8.54%
90	90.6	2.35%
95	95	2.06%
100	98.6	2.48%
105	68.8	3.77%
110	113.6	0.79%
115	117.2	2.17%
120	118.6	5.34%

4.1.4 Determining distance

The calibration curves were used to determine the distance to the target for an arbitrary measurement. First, assuming that the measured data had a random error with a Gaussian spread and a standard deviation $\sigma = rmse$, resulted in an uncertainty in distance for every calibration curve. For a given confidence (e.g. 2σ for 95 %), there was an interval within which the position could be determined as well as a total uncertainty in distance when all calibration curve comparisons were combined.

The data from the sequence 1 measurements on T54 were used to estimate the actual positions using the calibration curves (see Fig. 4.9). The estimation was done by minimising the sum of the square of the deviation from the calibration curve for all measurement points. The real distance, the estimated distance and the ratio of the minimum square sum for the estimated depth to the average over the whole range is listed in Tab. 4.1.4

The deviation is plotted in Fig. 4.10 and had a sine-shaped pattern. The uncertainties increases as the local minima or maxima coincided for the calibration curves, as expected. The deviation also increased with distance

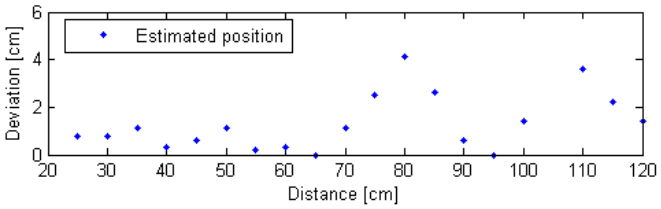

Figure 4.10: Deviation of the estimated position from the real position.

as the calibration curve amplitude decreases and approaches the noise level.

The average error of the estimated distance compared to the actual distance was 3.0 cm, or 1.3 cm when the point at 105 cm was excluded, where the incorrect minimum had been found. For a finial system, more work has to be put into comparing other local minima of similar magnitude and determining a minimum variation from each other. For this, the standard deviation of the data points from the calibration curve provided a good reference. E.g. 2 σ could be used to produce a 95% confidence interval as well as a confidence that the correct minima had been found.

4.1.5 Horizontal distance measurements

The horizontal position of a target could be determined in a similar fashion as for the depth measurements, by comparing measurements to a calibration curve. First, assuming that moving the target horizontally creates a standing wave pattern that varies with distance to the sensor, just as when varying the distance in depth, gave a curve $s = s(y)$, where y is the horizontal distance perpendicular from the concentric line. The curve s used in this section was related to the depth calibration curve $d(x)$, where x is depth, by $s(y) := d(\sqrt{X^2 + y^2})$, where X is the depth at which the target is moved horizontally. Then multiplying the difference of the curve s and the signal without target(s_0) by a function, $p(y)$ to take into account the effect of the shielding:

$$\Delta s = s - s_0, \tag{4.3}$$

$$signal = \Delta s p(y), \tag{4.4}$$

A constant shift, m, also had to be added, since the output voltage for the horizontal measurements were shifted from the depth measurements. The function that was fitted to the data was:

$$(s - s_0)p(y) + m \tag{4.5}$$

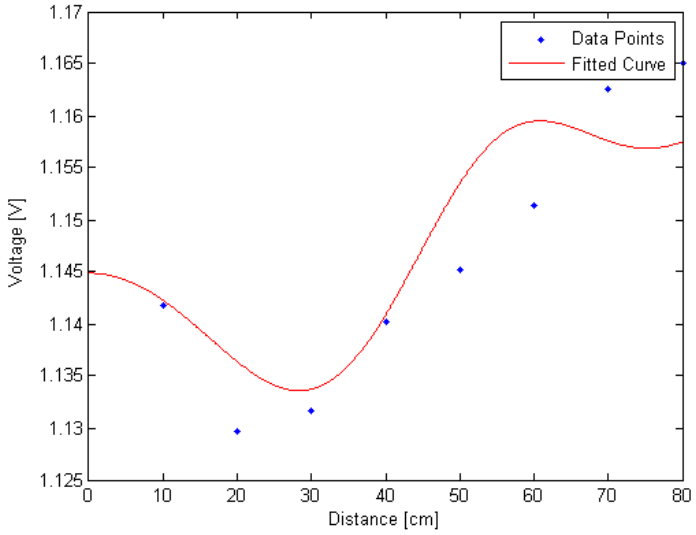

Figure 4.11: Fitted curve and data points for side measurements at 50 cm depth.

where *p(y)* is chosen to be a normal distribution centred around *x=0* with a standard deviation c:

$$p(y) = e^{-y^2/2c^2} \tag{4.6}$$

The model has been fitted to the sequence 2 measurements for the small antenna and T54 in Fig. 4.11. The standard deviation, c, for this measurement was 54.7 cm. This gives an indication of the field of view of the system, limited by the shielding.

The fit provided an indication that the horizontal measurements were proportional in magnitude to the corresponding depth measurements, with the magnitude decreasing as the target moved out of the field of view of the receiver. The shape of the target could be studied by moving the radar system horizontally, given knowledge of the depth.

4.2 Vertical Plane Measurements

Here, the measurement numbering refers to Ch. 3.1.7

The first vertical plane measurement had low resolution, but the standing wave patters could still clearly be seen in the contour map (Fig. 4.12). In the second measurement, a slight drift in voltage was observed. When

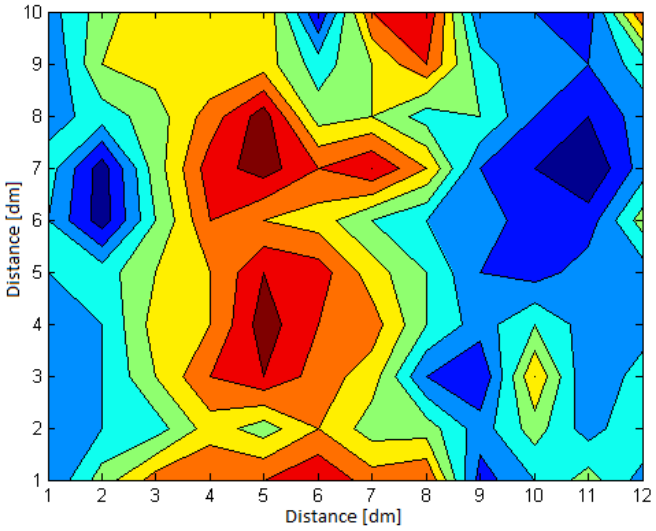

Figure 4.12: Vertical plane height map, measured without extra amplifier.

measuring the last point in the measurement series, there had been a 50 mV drift compared to the first point. Fig. 4.13 has been compensated for this 50 mV drift, assuming it was linear. In Fig. 4.13 the standing wave pattern can be seen in more detail due to the extra amplification.

These measurements can be compared to the standard deviation of the sideways measurements, 27.4 cm. It is of the same magnitude as the width of the red and yellow region in the middle of Fig. 4.13 corresponding to the target.

4.3 Snow Measurements

The purpose of the standing wave measurement in snow was to give an indication to weather or not the system could penetrate this medium. An electric wave travelling through snow would be heavily attenuated, and a system measuring only electric signals would therefore loose the ability to recognise a target signature. This is where one of the traits of the magnetic GPR can be noticed.

In Fig. 4.14, the measurement in snow is compared to the corresponding measurement in air. Due to the slightly different measurement systems in the two measurements the data is normalized to the square zero-level for comparison. The snow data points clearly follows the corresponding measurements for air.

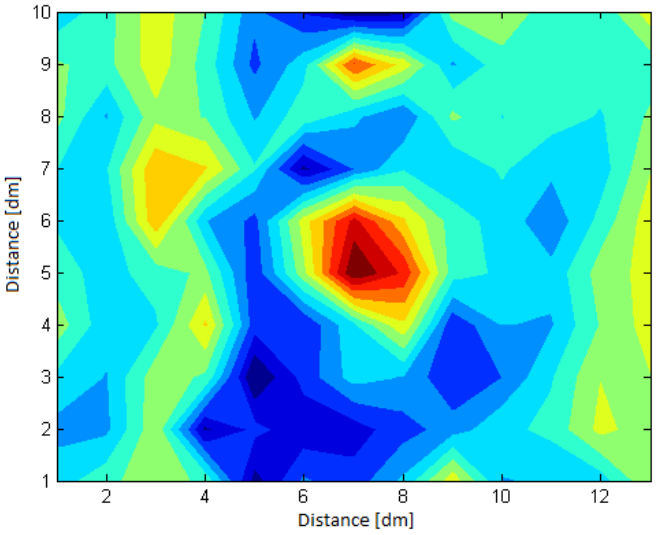

Figure 4.13: Vertical plane height map, measured with extra amplifier.

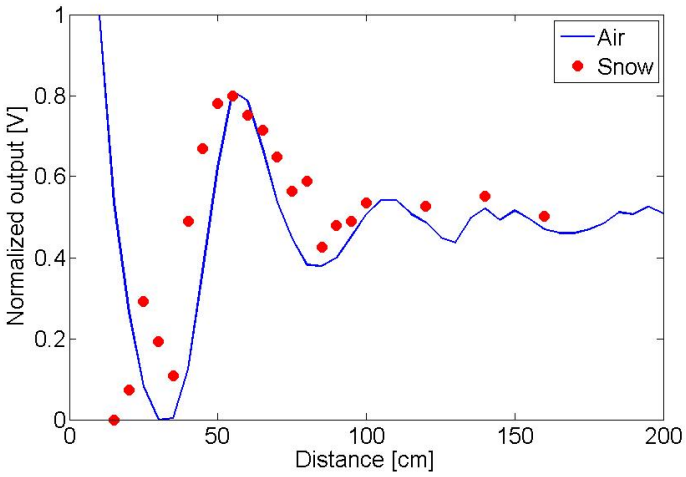

Figure 4.14: Standing wave measurements in snow.

4.4 Pulse Measurements

Looking at the pulse measurements with T54 at a distance of 150 cm (Fig. 4.16) and without target (Fig. 4.15), they appear more or less the same. Subtracting the two curves (see Fig. 4.17) confirms the suspicion that no clear shift can be observed where a shift of about 10 ns should be expected for a signal reflected at 1,5 meters.

The same result was achieved using the Mini-circuit logarithmic amplifier. It is fair to conclude that no pulse can be distinguished using the setup. There are many reasons why the setup worked less well for detecting pulses. First, the rise-time and length of the pulse was in the same order of magnitude as the travel time to the target and back again, meaning that the pulse is still transmitted when it starts to be detected. Major modifications would probably have to be done to the transmitter part of the system to make it perform satisfactory in pulse-mode.

Second, it is also unknown how much of the pulse that is actually radiated by the antenna. It should also be noted that the switch did not produce a proper pulse, but it can rather be described as a amplitude modulated signal with a carrier wave wavelength about 5 times shorter than the pulse length. On top of this, the pulse used is still being transmitted when the supposedly reflected pulse is being received.

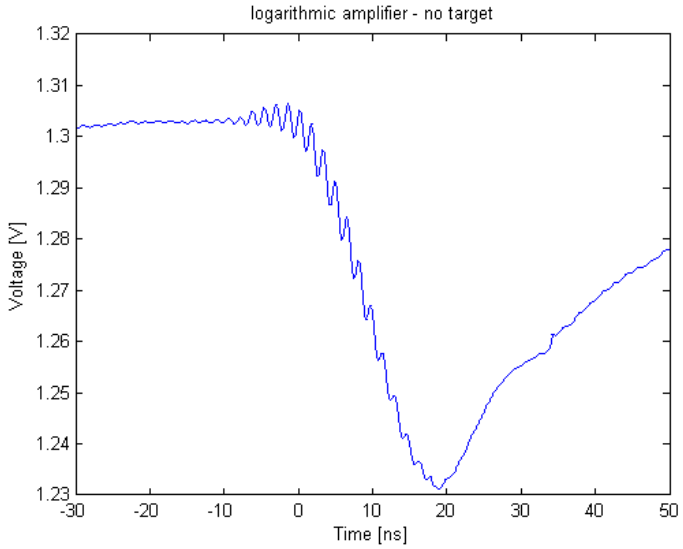

Figure 4.15: Pulse measurements with logarithmic amplifier and no target.

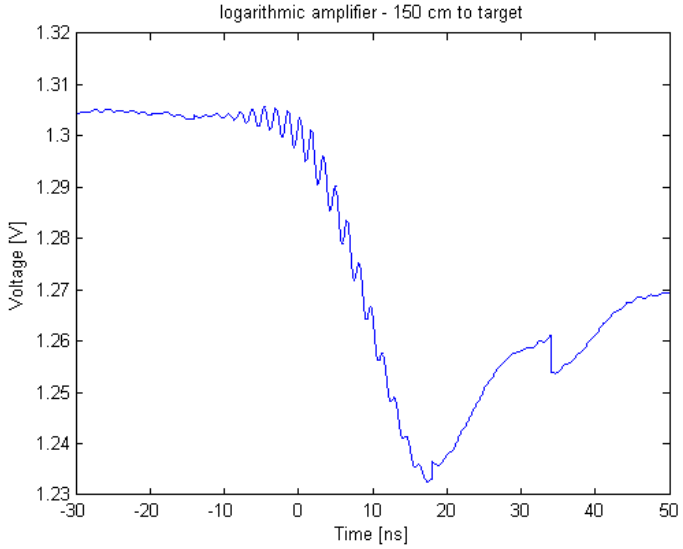

Figure 4.16: Pulse measurements with logarithmic amplifier and 150 cm to target (T54).

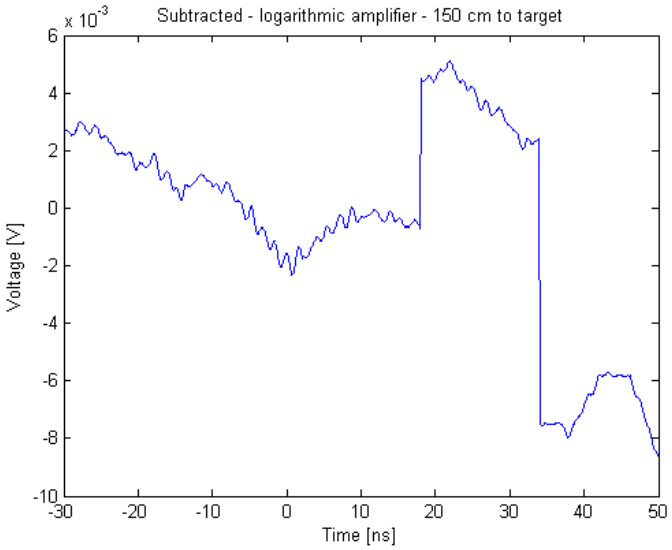

Figure 4.17: Difference between the pulse measurements with logarithmic amplifier and the measurements with no target. The discontinuities are a result of the interval recording of the data.

Chapter 5

Conclusion

The height contours from the vertical plane measurements (Fig. 4.13) are basically the same as one would get sweeping the radar system over an object buried under ground. The different standing wave patterns formed by each of the three orthogonal sine waves could then be used to determine the distance to target, using the statistically most likely position by minimizing the square root distance between the standing wave curves and the actual measurement for all three frequencies. The data would have to be normalized to the calibration curves, since the size, material and shape of the object is unknown. The normalization could be done by scaling all calibration curve linearly to it's real magnitude (the actual field magnitude, not the output voltage), using the same scaling parameter. The scaling parameter providing the smallest deviation would then be used.

The experiments and data analysis has provided useful quantifiable data regarding the system resolution and performance. The depth average error is 1.3 cm for the T54 target. Looking at Fig. 4.1 it can be observed that T54 have a high R^2 of about 0.8. For T27 it is close to 0. This means there is a greater spread in the data then from the calibration. Therefore, the depth error would increase fast as the diameter decreases. At its current form, the system can detect targets in the order of 50 cm diameter with reasonable accuracy. For the side direction, the system has a similar resolution as the distance varies. In addition to this the shielding blocks any target outside the coaxis, roughly with a Gaussian spread with standard deviation 27.4 cm. This gives an indication of the side resolution.

The pulse measurements proved unsuccessful. However, only pulse trains on shielded loop antennas were tested. Further research could be done using a better pulse generator where e.g. charged capacitors are used to generate the pulse. Other antennas could also be considered.

5.1 Applications

It has been shown that the radar system is effective at finding magnetic signatures at a depth of a few meters. This is a range comparable to many commercial systems [3]. One possible application could be archaeology where the archaeologist could survey a large area using the a small hand-held device. This would be made possible by the small size of the system. Current commercial systems are typically the size of a lawn mower [3], which would cause significant hindrance for the operator in rough terrain. The limiting factor, in terms of size, for the SDTM GPR is the antenna. One could potentially use smaller antennas. However, reducing the size of the shielded loop antennas would cause more attenuation of the signal and thus a reduced range. Further research could be done using other types of antenna, for example a horn antenna with higher directivity and more narrowband. The antennas could be fold-able or retractable for transportation purposes. The size of such an antenna would hardly cause any inconvenience in field use.

Another application of the SDTM GPR could be at construction sites, where possibly obsolete and inaccurate maps are the only way to avoid damaging buried water pipes and cables. A small GPR system could for example be mounted on the digging equipment.

5.2 Future research and development

However, there is still further development to be done before a working commercial system can be realized. Using a better pulse generator and a more appropriate antennas is necessary to fully evaluate the performance in the time domain. More reliable antennas have to be built, and other designs tested, for example a horn antenna with higher directivity. The noise in the system has to be further reduced, especially in the cables. A program to produce an actual image from the measured data and more advanced methods to determine the depth are also an important step towards a commercialization.

Acknowledgments

The following people have provided valuable assistance with this thesis project:

Ångström space technology center (ÅSTC)

Anders Persson, PhD student

Hugo Nguyen, Assistent professor

Johan Sundquist, Research engineer

Minh Nhut Tran, Research engineer

Greger Thornell, Associate professor

Henrik Kratz, Assistant professor

Swedish institute for space physics (IRF)

Lennart Åhlén, Principal research engineer

Jan Bergman, Researcher

A special thanks to my supervisor Anders Persson for giving comments on the report and guiding me through the project with patience.

Bibliography

[1] Åstc homepage: www.astc.material.uu.se. 2011-08-22.

[2] L. Karlsson A. Persson. Sdtm-workpackage 2: Req. spec. 2007.

[3] David Daniels. *Radar Handbook*, chapter 21. Ground Penetrating Radar. McGraw-Hill, 2008.

[4] P. T. Bellett et al. An investigation of magnetic antennas for ground penetrating radar. *Progress in Electromagnetics Research*, PIER 43:257–271, 2003.

[5] P. T. Bellett et al. A new magnetic antenna design for ground penetrating radar. In *D. Noon, Proceedings of the URSI-F Commission F Triennium Open Symposium.*, volume 1, pages 1–9. Ground Probe, 2004.

[6] A. Persson. Magnetoresistance and space. In *Digital Comprehensice Summaries of Uppsala Dissertations from the Faculty of Science and Technology 829*. 2011.

[7] Douglas H. Werner. An exact integration procedure for vector potentials of thin circular loop antennas. *IEEE transactions on antennas and propagation*, 44(2):157–165, February 1996.

Appendices

Appendix A

Calibration and measurement program

This program takes care of calibration of the measurement system and also perform the measurements themselves.

Program listing:

- - - - - - - - - - - - - - -

gprRun_logAmp.m

- - - - - - - - - - - - - - -

```
function gprRun_logAmp ()

%%  Program for the Ground penetrating Radar Projekt, ASTC
%   Author:         Mikael Blomqvist, Thesis student
%   Description:    Callibrates and runs the Experiment setup
%   Notes:
%   All communication with the Oscilloscope and the DAC is run through an
%   interface consisting of functions. The purpose is to be able to test
%   the program also when neither the Oscillsocope and/nor DAC is connected
%
%   !!IMPORTANT!!
%   This function is Called from a parameter file gprParam*.m that sets all
%   the constants in gprParam.mat

close all
clear all

% Check for opened Oscilloscope connections, then close them
if isempty(instrfind)
else
closeOsc(instrfind);
delete(instrfind);
end
```

```
% This user input file contains all the parametrs used by the program
load('gprParam.mat')

% Run calibration. Either real or simulated (for testing purposes)
% Checks if user want to run calibration, else, load old calibration
if calibrate
    % Checks if user want to simulate calibration
    if simCali
        polynomial = gprSimCali;
    else
        polynomial = gprRunCali;
    save(polynomialFile, 'polynomial')
    end
    disp('Finished calibrating, press key to continue')
    pause
else
    load(polynomialFile)
end

% Make measurement
i=0;
% Checks if user wants to make a measurement
if measure
    [ temp, n ]  = gprMeasure(polynomial, MEAS_FREQ, MEAS_NUM, SAMPLE_RATE);
    data = 0;
    data = temp(1:n);

    % Saves and plots the measurement
    dist = linspace(DIST_B,DIST_STEP*(n-1),n);
    save(MEAS_DATA_FILE, 'data', 'n','dist')
    plot(dist, data)
end

% plots the results of the calibration if the user wants to
if PLOT
    step = (VOLTAGE_END - VOLTAGE_START)/(NUM_INTERVALS-1);
    x = (VOLTAGE_START:step:VOLTAGE_END)';
    f = polyval(polynomial,x);
    plot(x,f,'o')
end

end

%% Calibration
%   - this function calibrates the measurement system and returns the
%   result as a vector with polynomial coefficients.
function [ p ] = gprRunCali( )

% This user input file contains all the parametrs used by the program
% Has to be loaded for every new function.
load('gprParam.mat')

% Load the DAC and set sample rate
ao = loadDAC(SAMPLE_RATE)
```

```
% Load Oscilloscope, obj1 can be used as a file
obj1 = loadOsc

% Sets step size for the DAC
step = (VOLTAGE_END - VOLTAGE_START)/(NUM_INTERVALS-1);

% TEST - Cycle through voltages
v = linspace(VOLTAGE_START, VOLTAGE_END, NUM_INTERVALS)';

% MAIN LOOP

    % Open the Oscilloscope for writing:
    fopen(obj1);

    % Reset the oscilloscope. It's now in a 'known state'
    fprintf(obj1, '*RST')
    % Set scale to autoscate for highest resolution
    fprintf(obj1, ':AUTOSCALE')

for i = 1:NUM_INTERVALS

    % This section makes the DAC output a voltage (i-1)*step
    x = (i-1)*step*ones(100,1);
    % Load data to DAC
    putdata(ao,x);
    % Repeat the output indefinately
    set(ao,'RepeatOutput',inf)
    % Starts the DAC
    start(ao);

    % Wait for the system to stabilize
    pause(PAUSE);

    % Instructs the Oscilloscope to measure the frequency
    fprintf(obj1, ':MEAS:FREQ?');

    % Reasds the measured frequency from Oscilloscope
    data = fread(obj1,11);

    % Saves data in a matrix
    d(i,:) = str2num(char(data)') ;

    %Stop the DAC
    stop(ao);

end

    %Disconnect Oscilloscope:
    fclose(obj1);

% Least square polynomial fit
if (NUM_INTERVALS < 5)
p = polyfit(v, d, NUM_INTERVALS-1)
else
```

```
    p = polyfit(v, d, 4)
end

stop(ao);

end

%% Sim Calibration
%   - Simulates the calibration for testing purposes
function [ p ] = gprSimCali( )

load('gprParam.mat')

% Main Program

step = (VOLTAGE_END - VOLTAGE_START)/(NUM_INTERVALS-1);

% TEST - Cycle through voltages
v = linspace(VOLTAGE_START, VOLTAGE_END, NUM_INTERVALS)';

% MAIN LOOP

for i = 1:NUM_INTERVALS

    % TEST
    data = (i-1)*step;

    d(i,:) = data ;

end

% Least square

% polynomanpassning
if (NUM_INTERVALS < 5)
p = polyfit(v, d, NUM_INTERVALS-1)
else
    p = polyfit(v, d, 4)
end

end

%% Measure
%   - measures the voltage from logarithmic amplifier with Oscilloscope
function [ data, n ] = gprMeasure( p, MEAS_FREQ, MEAS_NUM, SAMPLE_RATE)

%Note: Data cannot be loaded from external file since the function has
%subfunctions

% Load the instruments
ao = loadDAC(SAMPLE_RATE);
obj1 = loadOsc;

% Finds root of calibration polynomial (the wanted voltage), then creats a
```

```
% vector x to send to the DAC
answer = findRoot()
x = answer*ones(100,1);

% Load data to DAC, and repeat output
DACputdata(ao, x);
DACset(ao,'RepeatOutput',inf)

% Start DAC
DACstart(ao)

% Connect to Oscilloscope
openOsc(obj1)

% Sets up Oscilloscope parameters
% First reset to produce predictable results
send2Osc(obj1, '*RST')
% Time range (10 times time/div)
send2Osc(obj1, ':TIM:RANG 10e-3')
% Chan1 range (8 times V/div)
send2Osc(obj1, ':CHAN1:RANG 800e-3')
% Use FFT
send2Osc(obj1, ':FUNC:OPER FFT')

% Give user time to adjust settings additionally
pause

getVmax;
% Set center of FFT
send2Osc(obj1, ':FUNC:CENT 490e6')
% Set FFT frequency span
send2Osc(obj1, ':FUNC:SPAN 2e9')
% dB / screen (8 times dB / div)
send2Osc(obj1, ':FUNC:RANG 16e1')

% Give user time to adjust settings additionally
pause

% Measure max amplitude for MATH chanel (dB)
    % create big enough vector to make data handling faster
    data = zeros(1,20);
    k = 1;
    flag1 = false;
    readStr
    % 'Press enter to continue, type q to quit, d to delete, e to edit, d to display

    while (string2 ≠ 'q')

    if string2 == 'd'
        if k ≥ 2
            disp('last data deleted')
            k = k - 1;
        else
            disp('already at no1')
```

```
        end
        flag1 = true;
    end
    if string2 == 'r'
        restartNum = input('restart from:, a to abort ' ,'s')
        if restartNum ≠ 'a'
            k = str2num(restartNum);
            disp('num2str(k)')
        else
            disp('aborted')
        end
        flag1 = true;
    end
    if string2 == 'e'
        editNum = input('edit number:, a to abort ' ,'s')
        if editNum ≠ 'a'
            data(str2num(editNum)) = getVmax;
            disp('number edited');
        else
            disp('aborted')
        end
        flag1 = true;
    end
    if string2 == 'l'
        disp([num2str(k-1) 'data entries'])
        data'
        flag1 = true;
    end

    if flag1 == false
        data(k) = getVmax;
        k = k + 1;
    else
        flag1 = false;
    end
    readStr;
    end

    n = k-1;

closeOsc(obj1)
DACstop(ao);

    function readStr
        string1 = ['Number: ' num2str(k) ' '];
        string2 = input(string1 ,'s');
        if isempty(string2)
            string2 = 'c';
        end
    end

    function answer = findRoot()
        % Finds the root of the polynomial
        q = p - [0 0 0 0 MEAS_FREQ];
```

```
        r = roots(q);

        temp = size(r);
        n = temp(1,1);

        answer = 0;
        for i = 1:n
            if isreal(r(i))
                if (r(i)>0) && (r(i)<10)
                    answer = r(i);
                end
            end
        end
    end

    function averageVmax = getVmax
         averageVmax = 0;

         for i = 1:MEAS_NUM
             temp = readOsc(obj1, ':MEAS:VAV?');
             Vmax = str2num(char(temp)') ;
             averageVmax = averageVmax + Vmax;
         end
         averageVmax = averageVmax / MEAS_NUM;
    end

end

%% Functions to create interface to Oscilloscope and DAC

function ao = loadDAC(SAMPLE_RATE)

load('gprParam.mat', 'simDAC')
if simDAC
    ao = 0;
    return
end

DACreset
%Create analog output object ao
ao=analogoutput('agilentu2300',0);
%Add hardware channels to ao
addchannel(ao, 0);
% Set sampling rate
set(ao,'SampleRate',SAMPLE_RATE);

end

function obj1 = loadOsc

load('gprParam.mat', 'simOsc')
if simOsc
    obj1 = 0;
    return
```

```
end

% Create a VISA-USB object.
obj1 = instrfind('Type', 'visa-usb', 'RsrcName', 'USB0::0x0957::0x1755::MY48150023::0::INSTR'

% Create the VISA-USB object if it does not exist
% otherwise use the object that was found.
if isempty(obj1)
    obj1 = visa('Agilent', 'USB0::0x0957::0x1755::MY48150023::0::INSTR');
else
    fclose(obj1);
    obj1 = obj1(1)
end
end

function openOsc(obj)
load('gprParam.mat', 'simOsc')
if simOsc
    return
end
    fopen(obj);
end

function closeOsc(obj)
load('gprParam.mat', 'simOsc')
if simOsc
    return
end
    fclose(obj);
end

function send2Osc(obj, s)
load('gprParam.mat', 'simOsc')
if simOsc
    return
end
    fprintf(obj, s)
end

function out = readOsc(obj, s)
load('gprParam.mat', 'simOsc')
if simOsc
    out = '0';
    return
end
    fprintf(obj, s)
    out = fread(obj);
end

function DACputdata(ao, x)
load('gprParam.mat', 'simDAC')
if simDAC
    return
end
```

```
    putdata(ao,x);
end

function DACset(ao,s,num)
load('gprParam.mat', 'simDAC')
if simDAC
    return
end
    set(ao,s,num)
end

function DACstart(ao)
load('gprParam.mat', 'simDAC')
if simDAC
    return
end
    start(ao);
end

function DACstop(ao)
load('gprParam.mat', 'simDAC')
if simDAC
    return
end
    stop(ao);
end
```

Appendix B

Parameter file for Calibration and measurement program

This program sets the parameters for calibration and then calls gprRun_logAmp.m to perform the calibration. When gprRun_logAmp is called using these parameters, the Oscilloscope must be connected, but not the DAC. (simOsc = 0, simDAC = 1)

Program listing:

- - - - - - - - - - - - - - - -

gprParam.m

- - - - - - - - - - - - - - - -

```
%% Parameters

calibrate       = 0;
measure         = 1;
polynomialFile  = 'gprPoly_standard.mat';
simCali         = 0;
simMeasure      = 0;

% DAC
simDAC          = 1;        % the voltage was set manually, no DAC availabel at measurement t
SAMPLE_RATE     = 1000;
VOLTAGE_START   = 0;
VOLTAGE_END     = 10;

% Calibration
NUM_INTERVALS   = 21;
PAUSE           = 0.05;
PLOT            = 0;
```

```
% Oscilloscope
simOsc          = 0;

% Measurement - specific parameters for all measurements
% These were changed to relevant values for each run
MEAS_FREQ       = 490.2e6;
MEAS_NUM        = 20;
MEAS_DATA_FILE  = ['../Data/measurement_101130_1_' num2str(MEAS_FREQ/1000) 'kHz_#_#'
% the variable 'dist' will begin from DIST_B and increase in steps of
% DIST_STEP
DIST_B          = 10;
DIST_STEP       = 5;

% polynomial = 1.0e+008 * [-0.0002 0.0033 -0.0189 0.3340 2.4388];
% save('gprPoly.mat','polynomial');
save('gprParam.mat')

% Call gprRun
gprRun_logAmp()
```

Appendix C

Parameter file for calibration

This program sets the parameters for calibration and then calls gprRun_logAmp.m to perform the calibration. When gprRun_logAmp is called using these parameters, the Agilent DAC and the Oscilloscope must be connected.

Program listing:

- - - - - - - - - - - - - - -

gprParam_Calibrate.m

- - - - - - - - - - - - - - -

```
%% Parameters

calibrate       = 1;
measure         = 0;
polynomialFile  = 'grpPoly_calibration';
simCali         = 0;
simMeasure      = 0;

% DAC
simDAC          = 0;
SAMPLE_RATE     = 1000;
VOLTAGE_START   = 0;
VOLTAGE_END     = 10;

% Calibration
NUM_INTERVALS   = 21;
PAUSE           = 0.05;
PLOT            = 1;

% Oscilloscope
simOsc          = 0;

% Measurement
MEAS_FREQ       = 0;
MEAS_NUM        = 4;
MEAS_DATA_FILE  = ['measurement' num2str(MEAS_FREQ/1000) 'kHz'];
```

```
% the variable 'dist' will begin from DIST_B and increase in steps of
% DIST_STEP
DIST_B          = 10;
DIST_STEP       = 5;


% polynomial = 1.0e+008 * [-0.0002 0.0033 -0.0189 0.3340 2.4388];
% save('gprPoly.mat','polynomial');
save('gprParam.mat')

gprRun()
```